PHYSICAL REVIEW B VOLUME 36, NUMBER 9 15 SEPTEMBER 1987-II

Core-level binding-energy shifts, thermodynamic predictions, and morphologies for metal-Si and metal-Ge interfaces

M. del Giudice, J. J. Joyce, and J. H. Weaver
Department of Chemical Engineering and Materials Science, University of Minnesota, Minneapolis, Minnesota 55455
(Received 4 March 1987)

High-resolution core-level photoemission results show two or more distinct reacted chemical species for a wide variety of metal-Si and metal-Ge interfaces. Assuming that the first reacted species at the interface have ~50 at. % Si (or Ge) and the second species are solid solutions of Si (or Ge) in metal matrices, we find reasonable agreement between calculated and experimental chemical shifts. These analyses allow correlation between the reaction products observed at metal-semiconductor interfaces and the bulk thermodynamic properties of the constituents. These results are in agreement with those obtained from a morphological model for evolving interfaces developed by Butera, del Giudice, and Weaver.

INTRODUCTION

In the last decade, a large amount of experimental work has been done to characterize and understand metal-semiconductor interfaces.[1,2] Today, it is recognized that reacted interfaces are the rule rather than the exception. Indeed, high-resolution core-level photoemission has identified distinct chemical shifts in the semiconductor atomic core levels which are indicative of reaction.[3,4] The intriguing chemical and physical processes observed for these metastable systems are ultimately responsible for the complex morphologies of extended interfaces.[5,6] These results have a direct impact on thin-film technologies and microelectronic device fabrication.[7,8]

Several qualitatively different phenomena occur when metal adatoms are deposited onto semiconductor surfaces.[9] In some cases, adatom aggregation and island formation is observed because the interaction between metal atoms is stronger than interaction with the substrate. In others, layer-by-layer growth (possibly epitaxial) is observed.[10-15] Very frequently, however, there is substrate disruption and room-temperature intermixing.[16-18] Interestingly, these reactive systems also exhibit differences at low coverage (0–2 ML) related to adatom clustering as a precursor stage of reaction, on the one hand, and sudden reaction of the impinging metal atom, on the other.[19-21]

Once initiated, reaction is controlled by atomic diffusion as semiconductor atoms out-diffuse through the overlayer, probably via grain boundaries, to reach the reaction sites.[22,23] This appears to be the case for the transition-metal and rare-earth-metal overlayers. As metal deposition continues, the reacted layer thickens and it becomes an increasingly efficient diffusion barrier. Hence, the number of semiconductor atoms available for continued reaction on the metal side of the diffusion barrier decreases and the growing layer converges to a metallic film. In contrast, different overlayer morphologies are observed when the metal atoms are the diffusing species,[24] as for the case for Al,[25] some noble,[26,27] and the near-noble metals.[28,29] Some of these metals (Cu, Pt, Pd) are characterized by extended interdiffusion with the substrate and a thin solid-solution (or segregated) layer is sometimes formed at the surface (Au, Pd, Cu). Al, which exhibits limited intermixing with the substrate, appears to be the exception.

Insight into the growth characteristics of these systems can be gained through analysis of high-resolution core-level photoemission results. These photoemission spectra are obtained by following the changes in line shape of the Si 2*p* and Ge 3*d* core levels during the evolution of the interface. Subsequent quantitative line-shape decomposition of the core emission makes it possible to chart the growth and decay of each of the reaction products at the interface within the probed region. These intensities (termed attenuation curves) give information about interface morphologies and, less directly, the average stoichiometries of the species which form.[30,31] As we will show here, the chemical shifts are also directly related to the heats of formation (or solution) of the respective species, and these give independent insight into interface constituents and morphology.[32]

In this paper, we discuss the origin of the Si 2*p* and Ge 3*d* chemical shifts for simple-, transition-, noble-, and rare-earth-metal overlayers. We focus on the two reacted species which have been observed during interface formation.[33] From spectroscopic information and modeling of the morphological development of the interface, these have been identified as silicide or germanide phases and solid solutions.[30] Starting from these observations, we use a thermodynamical model to correlate the composition of the reaction product with the measured chemical shifts. Similarities and differences for a variety of interface systems will be examined, and the limitations of the model will be discussed. The major conclusions of this paper are (a) chemical shifts observed at metal-semiconductor interfaces can be explained in terms of compound or solution formation; (b) the first reacted components exhibit chemical shifts which are consistent with the formation of a compound having

 ©1987 The American Physical Society

~50 at. % Si or Ge; (c) the final component can be described as a solid solution, in agreement with intensity studies; (d) the chemical shifts for these two components show analogous behavior, suggesting that morphological and crystal structure differences in the reacted films play a secondary role in determining the chemical shift.

EXPERIMENTAL RESULTS

In Fig. 1 we show typical core-level photoemission spectra for a reactive transition-metal–Si interface, in this case for Sc/Si(111)2×1.[34] These results show the evolution of the Si 2p core level as a function of metal coverage Θ. Analogous spectra have been obtained for the other systems under review here. These results and those for the other materials were obtained by cleaving the semiconductor *in situ* at pressures in the 10^{-11} Torr range, characterizing the quality of the cleave with core-level and valence-band photoemission, and depositing controlled amounts of metal at pressures below $(2-3)\times 10^{-10}$ Torr, from degassed sources, are generally ~30 cm from the target. Typical deposition rates were ~1 Å/min. All of the results to be discussed here were obtained with room-temperature substrates.

The results of Fig. 1 show the onset of reaction at low coverage, as indicated by the low-binding-energy shoulder for $\Theta \sim 1$ monolayer (ML). This reacted feature grows with coverage as the substrate is disrupted and the silicide forms. With higher coverage, a second reaction product appears at lower binding energy relative to the first. By $\Theta \sim 5$ ML, emission from the substrate is no longer visible and the second reaction product is dominant. Results obtained with other photon energies give complementary information because of corresponding changes in the photoelectron mean free path (i.e., probe depth). Core-level line-shape decomposition makes it possible to determine the component-specific behavior.

In Fig. 2 we show the attenuation curves for Sc/Si(111)2×1 as determined from the spectra of Fig. 1 (Fig. 2, bottom panel) and for Ti/Si(111)2×1 (top panel). For the Sc/Si interface, the substrate emission decreases rapidly with coverage, the first reaction product grows and contributes a maximum amount at $\Theta = 3$ ML, and the emission at high coverage is predominantly due to the second product. Analogous behavior can be observed in the top panel for Ti/Si(111) where, in addition to the already mentioned reacted components, a third species is present in the ultralow-coverage region (1–2 ML).[35] This species has been identified as a Si-rich phase that develops at the interface between the substrate and the reacted region. The resulting graded interface therefore has a semiconductor-rich species which forms first, followed by a solid solution as the final step leading to a pure metallic film. Once formed, these phases coexist in a nondestructive way in the absence of changes in temperature. In the coverage range where

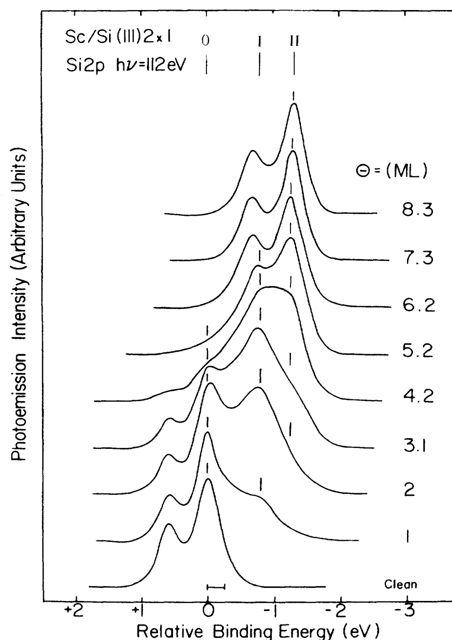

FIG. 1. Si 2p energy distribution curves (EDC's) measured at $h\nu = 112$ eV for Sc/Si(111). The EDC's are normalized to emphasize line-shape changes. A band-bending change of 250 meV is achieved by 1 ML. Two reacted components (labeled I and II) are observed, together with the substrate (labeled 0).

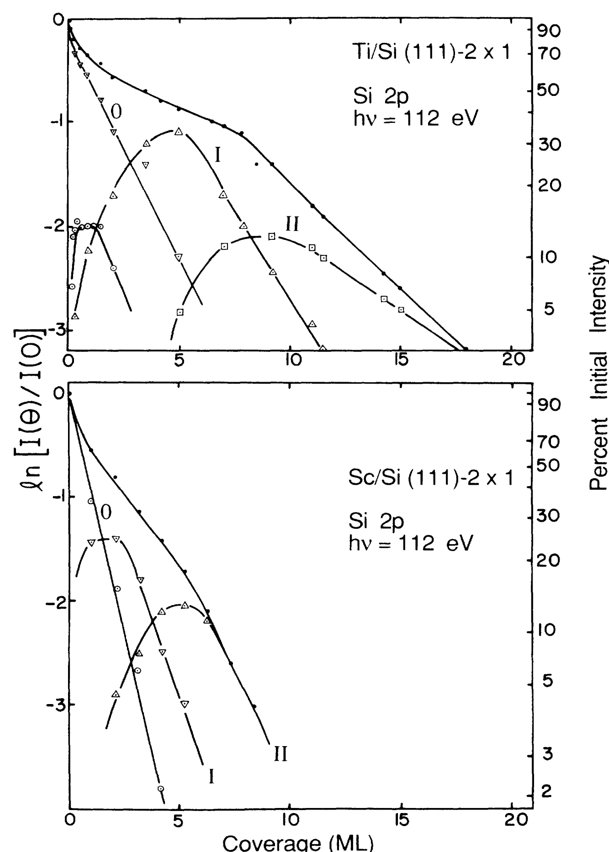

FIG. 2. Attenuation curves, $\ln[I(\Theta)/I(0)]$, vs coverage for Ti/Si (top panel) and Sc/Si (bottom panel) showing the total and component specific attenuation. The notation 0,I,II is the same as that of Fig. 1 and the tables.

transition from one phase to the next occurs, a thermodynamic lever rule can be applied, as discussed in detail by Butera *et al.*[30]

In general, the first Si $2p$ or Ge $3d$ component corresponds to a silicide or germanide having 50–60 at. % Si or Ge.[30,34–38] The line shape of the silicide or germanide is broader than that of the substrate because of slightly inequivalent atomic configurations, but its energy centroid is a constant. The second (full) component which grows at higher metal coverage is characterized by a line shape which usually sharpens with coverage and a binding energy which shifts to reach a saturation line. In our morphological modeling we (and others) have interpreted this behavior as evidence of solid-solution formation with semiconductor atoms completely coordinated by metal atoms.

In Tables I and II we summarize the observed core-level shifts (CLS's) for a wide range of metal-Si and metal-Ge interfaces. Each CLS is measured relative to the substrate core-level position with account taken for band-bending changes. Since relative barrier heights vary by 0.05–0.25 eV, there is a small error introduced by referring the CLS's to the pinned substrate. In the fifth column of each table we show the differences in Pauling electronegativity, ΔX, for these metal-semiconductor couples.[39] In the sixth column we report the number of reaction-induced components, N_c. When three components are detected, the CLS's refer to the last two observed with metal coverage. For Yb/Si (Ref. 40) and Cr/Si (Ref. 31) the Si $2p$ spectra were not well resolved, and we could estimate only the asymptotic value for the final component. From Tables I and II we can conclude that the signs of the observed chemical shifts follow the differences in Pauling electronegativities of the interface constituents. A more detailed analysis of the results in Tables I and II shows that there is also a dependence of the CLS on the electronegativity.

In Fig. 3 we present the observed CLS's for different metal overlayers on cleaved Si(111) (circles) and Ge(111) (squares) plotted against the Pauling-electronegativity difference between the metal and the semiconductor. The solid symbols correspond to the reacted silicides or germanides which dominate in the intermediate-coverage range, analogous to those shown in Fig. 1. Quantitative analysis of the attenuation curves indicates a semiconductor content of 50±5 at. % for Ce/Ge (Ref. 36), Ti/Si (Ref. 35), and Sc/Si (Ref. 34); 60±5 at. % for Ce/Si (Ref. 30), V/Ge (Ref. 30), and Co/Si (Ref. 37); and 40–50 at. % for Pd/Si (Ref. 38). The dependence of the CLS of component I on the electronegativity difference can be described with an *S*-shaped curve in Fig. 3. The results of Fig. 3 show a linear dependence of the CLS on the electronegativity difference for the transition metals, a saturation of the CLS for the rare-earth metals, and an analogous saturation for the noble (Au) and near-noble metals (Pt and Pd) on the opposite side of the electronegativity scale. Likewise, the open symbols of Fig. 3 which refer to CLS's for component II can also be fit by an *S*-shaped curve, shifted ~0.4 eV relative to that of the silicides or germanides.

Two important points follow from the data presented in Fig. 3. First, a common functional dependence is observed for both the solid solution and the ~50% phase, suggesting an underlying general mechanism which describes phase formation for metal-semiconductor interfaces. Second, the observed behavior for reactive interfaces allows us to predict the chemical shifts and to correlate the empirical composition (i.e., a chemical pa-

TABLE I. Experimental core level shifts (CLS's) for the Si $2p$ levels observed for different metal overlayers on Si(111)2×1. All CLS values are in eV and are referred to the pinned substrate. The first component (I) is associated with a phase with ~50 at. % average Si content. The second phase (II) is a solid solution. In the fourth column we show the doping of the Si substrate for the different junctions. Differences in Pauling electronegativity between metal and semiconductor are shown in the fifth column. Finally, in the sixth column we report the total number of observed CLS components. Where more than two components are observed, the values reported are the last two detected during interface evolution.

Metal	Experimental CLS (eV) I	II	Si type	ΔX Pauling electronegativities	N_c	Ref.
Au	+0.60		*p*	+0.64	1	26
Al		−0.73	*p*	−0.29	1	25
Ce	−0.66	−1.20	*n*	−0.78	2	18
Co	+0.30	−0.40	*n*	−0.02	2	37
Cr		−0.30	*n*	−0.25	a	31
Cu	+0.20	−0.20	*n*	0.00	2	This work
Gd	−0.70	−1.20	*n*	−0.70	2	54
Pd	+0.68	+0.25	*n*	+0.30	2	38
Pt	+0.70		*n*	+0.38	1	29
Sc	−0.80	−1.25	*n*	−0.54	3	34
Sm	−0.85	−1.30	*n*	−0.73	2	55
Ti	−0.65	−1.15	*n*	−0.36	3	35
V	−0.30	−0.86	*n*	−0.28	2	This work
Y	−0.80	−1.25	*n*	−0.68	2	This work
Yb		−1.25	*n*	−0.80	a	56

[a]Only the asymptotic value of the chemical shift is taken into account due to the poor resolution of the results.

TABLE II. Experimental CLS's for the Ge 3d core level observed for interfaces with Ge(111)2×1. The different columns have the same meaning as those of Table I.

Metal	Experimental CLS (eV) I	Experimental CLS (eV) II	Ge type	ΔX Pauling electronegativities	N_c	Ref.
Au	+0.75	+0.25	n	+0.53	2	49
Ce	−0.9	−1.30	n	−0.89	3	36
Cr	−0.5	−1.00	n	−0.35	2	57
Cu	+0.2	−0.25	n	−0.10	2	27
Sm	−0.63	−1.00	n	−0.84	2	58
Ti	−0.6	−1.15	n	−0.47	2	This work
V	−0.5	−0.95	n	−0.35	2	19
Yb	−1.0	−1.50	n	−0.91	3	50

rameter) to the spectroscopically observed shift in the semiconductor core level.

DISCUSSION

In principle, the functional dependence of the CLS on electronegativity difference could be described in terms of transferred charge, as implicit in the concept of electronegativity, but such an approach is ambiguous.[41,42] In particular, the amount and direction of charge transfer is not well defined for bonding character that is not strictly ionic. Moreover, difficulties in calculating the relaxation energies[43] and the Madelung potentials[44] for complex (and sometimes unknown) structures makes this approach undesirable. Instead, we will relate the observed CLS's to thermodynamic properties.

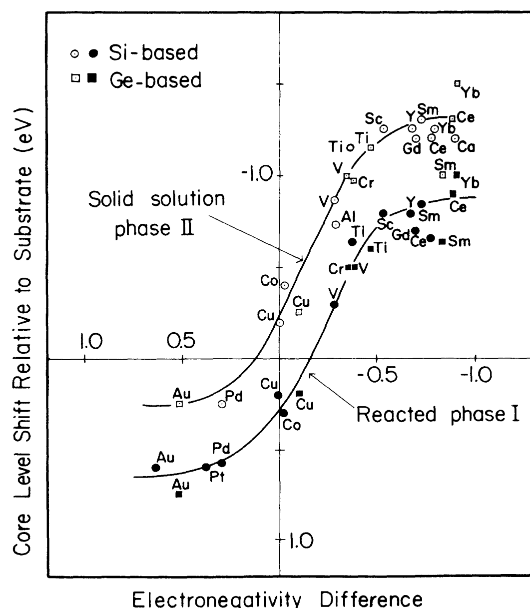

FIG. 3. Experimental CLS's for Si 2p and Ge 3d observed for metal overlayers on cleaved Si(111)2×1 and Ge(111)2×1 surfaces as a function of the difference in Pauling electronegativity between the metal and the semiconductor. The two S-shaped curves show similar behaviors for the solid solution phase and the first reacted phase.

Mårtensson and Johansson[45] recently showed that photoemission chemical shifts in the core lines for A atoms in an environment constituted by B atoms can be correlated to the heats of formation of the species considered. Using a Born-Haber cycle and assuming that the fully screened, core-ionized Z^* atom can be replaced by the neutral $Z+1$ atom, the chemical shift is given by the difference between thermodynamic quantities. This approach has been extended to metallic compounds by Verbeek, and we will refer to his treatment in the following.[46]

The chemical shift of an atom A with atomic number $Z(A)$ in a binary AB phase relative to the pure material A can be written as

$$\Delta E(A)=f(A;A)H_f(A(Z+1);A(Z)) +f(A;B)H_f(A(Z+1);B) -f(A;B)H_f(A(Z);B) -H_s(A(Z+1);A(Z)) , \quad (1)$$

where $f(A;B)$ are environment factors defined as the fraction of B atoms around an A site, $H_f(A;B)$ is the heat of formation of the binary alloy AB, and H_s is the heat of solution of A in B. If the phase is a solid solution of A (the solute) in B (the solvent), then Eq. (1) becomes

$$\Delta E(A)=H_s(A(Z+1);B)-H_s(A(Z);B) -H_s(A(Z+1);A(Z)) . \quad (2)$$

In Eq. (2) only the heats of solution are used such that $H_s(A(Z+1);B)$ is the heat of solution for atoms A with atomic number $Z+1$. To calculate these quantities for silicon-based systems, we use the properties of phosphorus; likewise, arsenic is the $Z+1$ partner for germanium.

For the silicides and germanides we assume for the sake of simplicity that all the compounds have the CsCl structure and have a semiconductor content of 50 at. %. With these approximations, Eq. (1) becomes

$$\Delta E(A)=H_f(A(Z+1);B)-H_f(A(Z);B) -H_s(A(Z+1);A(Z)) , \quad (3)$$

where the heats of formation are now included and the results should show the trends in the CLS's.

Although it is possible, in principle, to calculate chemical shifts using experimental values for thermodynamic quantities, few of these values have been measured. Approximate values for the heats of formation and solution can be calculated using the semiempirical Miedema model.[47,48] Since the Miedema model for solutions assumes that the alloys are liquids, there will be differences arising from elastic strain energy and crystal structure. Moreover, further approximations must be considered when there is *p-d* hybridization, as will be discussed. The Miedema model works best when at least one of the two constituents is a transition metal. For elements like P or As, an imaginary metallic state must be introduced, and one should expect only qualitative agreement between the experimental CLS's and the calculations. In particular, the heat of solution for P in Si or As in Ge are always present in both Eqs. (2) and (3), and these quantities enter as additive constants for all the chemical shifts considered. The Miedema scheme gives values of −318 and −1 kJ/mole, respectively, for these two quantities. For P-Si, the Miedema value is too large, probably because of the above-mentioned difficulties in considering a metallic P-Si liquid alloy, and we have normalized the constant $H_s(\mathrm{P;Si}) = -48$ kJ/mole to the experimental results. To our knowledge, no experimental value is available in this case. No other adjustment of the calculated values of metal alloys has been done.

In Tables III and IV we report the calculated heats of formation and solution for metal-silicon and metal-germanium phases together with the calculated CLS's using Eqs. (2) and (3). The sign convention is a binding-energy increase and a positive CLS for exothermic reactions involving negative heats of formation. To simplify the comparison between the predicted and the observed CLS's, we plot in Fig. 4 the results of Tables I and III. The arrangement of metal species corresponds to increasing electronegativity differences, except for Al which represents a particular case, as will be discussed. The solid circles are the experimental values and the open circles are the calculated values. The top panel shows qualitative agreement for solid-solution phases involving Si embedded in the metals. In particular, the sign of the shifts is correct, and the correspondence between the experimental and calculated trends is best for the refractory and rare-earth metals. The bottom panel summarizes analogous results for the metal-silicide phases where the calculations assumed the CsCl structure. Even with this first-order approximation, the experimental trend is reproduced. There is an almost linear dependence of chemical shift on electronegativity differences for the refractory metals and the dependence is very small at both ends for the rare-earth and noble metals.

In Fig. 5 we summarize the experimental and predicted CLS's for metal-Ge systems. Although the experimental trend for Ge interfaces is similar to those involving Si, the Miedema model fits the results only approximately. As for Si-based interfaces, the biggest discrepancies are observed for Au and Yb overlayers. For Au, both the solid solution and the intermixed phase have positive shifts where the calculations predict negative shifts.[49] On the other hand, the interpretation of the Au/Ge results has not been free of pitfalls and the presence of surface-segregated Ge cannot be excluded. By analogy with the calculated Si results, we should expect positive shifts. For Yb/Ge, we suspect that the experimental values of Ref. 50 are overestimated.

In Fig. 6 we show the correlation between the calculated CLS's (ordinate) and the experimental CLS's (abscissa) to show the validity of the assumptions on which the model is based. The open circles represent the solid solutions and the solid circles the *AB* metal-

TABLE III. Calculated values for Si 2*p* CLS's for the first reacted phase (I) and the final solid solution (II). Also shown are the heats of solution (second column) and heats of formation (third column) computed with the Miedema model.

Metal	ΔH_f [a] (kJ/mole)	ΔH_s [b] (kJ/mole)	Calculated CLS (eV) I	II
Au	−7.7	−48	+0.60	+0.65
Al	−104.0	−232	−0.10	−0.60
Ce	−76.0	−181	−0.48	−1.30
Co	−31.0	−91	−0.18	−0.02
Cr	−30.0	−87	0.00	−0.66
Cu	−1.3	−40	+0.10	−0.18
Gd	−78.0	−186	−0.50	−1.36
Pd	−57.0	−145	+0.40	+0.58
Pt	−55.0	−138	+0.60	+0.70
Sc	−79.0	−202	−0.50	−1.50
Sm	−78.0	−181	−0.50	−1.36
Ti	−74.0	−190	−0.40	−1.45
V	−46.0	−128	−0.22	−1.00
Y	−78.0	−186	−0.5	−1.35
Yb	−37.0	−108	−0.32	−1.10

[a]Calculated for a compound A_xB_{1-x} ($x = 0.5$) and a CsCl structure.
[b]Calculated in conditions of solubility limit.

TABLE IV. Calculated values for Ge 3d core-level shifts (CLS's). Same convention as in Table III.

Metal	ΔH_f [a] (kJ/mole)	ΔH_s [b] (kJ/mole)	Calculated CLS (eV) I	II
Au	−7.00	−36.0	−0.18	−0.05
Ce	−89.00	−202.0	−0.50	−0.85
Cr	−13.00	−28.0	−0.36	−0.82
Cu	−2.00	−30.0	−0.20	−0.28
Sm	−88.00	−204.0	−0.50	−0.90
Ti	−64.00	−159.0	−0.44	−1.00
V	−32.00	−80.0	−0.35	−0.82
Yb	−60.00	−1.52	−0.35	−0.60

[a] Calculated for a compound A_xB_{1-x} ($x=0.5$) and a CsCl structure.
[b] Calculated in conditions of solubility limit.

semiconductor compounds. The solid line represents a perfect correlation between experiment and theory. Contributions from Yb or Au are excluded since they are the most ambiguous. Despite the scattering of the experimental points, the theoretical line represents a good fit to the results.

There are several possible sources of error that can account for the quantitative scattering. First, there are experimental errors in determining CLS's. For example, although the shifts are referred to the pinned substrate, different groups have adopted different procedures for line-shape analysis and an error of ±0.1 eV is not unreasonable. Second, there is an error of 20% built into the calculations for the heats of formation or reaction as obtained with the Miedema scheme.[48] A more fundamental error lines in the origin of the calculated heats of formation for an AB compound where A is a d-band metal and B is an s-p element.[41] A compound of calculated and measured heats of formation has been reported by Miedema.[51]

Two effects determine the qualitative behavior of the

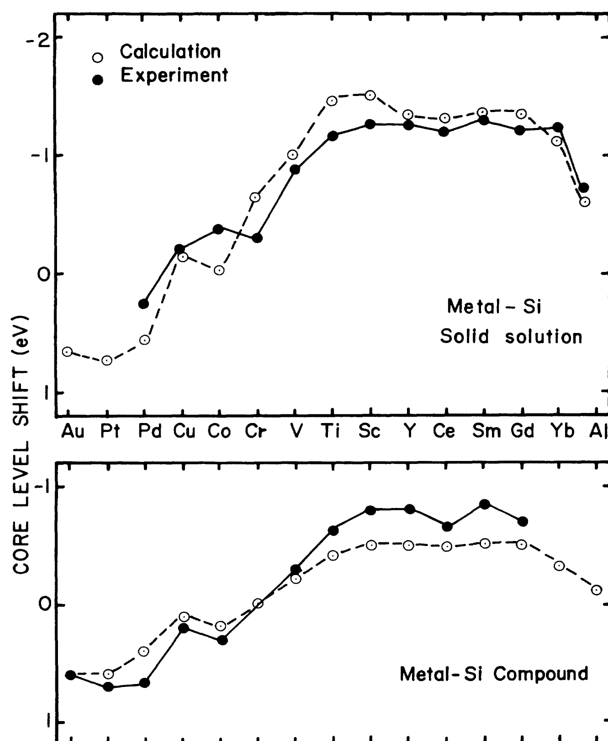

FIG. 4. Experimental and calculated Si 2p CLS's for different metal overlayers. The top panel summarizes the trends for the solid solution phase. The bottom panel shows analogous results for the first reacted phase (calculations based on CsCl structure and a 50 at. % Si content). Good agreement is observed. The Al/Si case is reported at the right-hand side since its morphology is substantially different from the other systems.

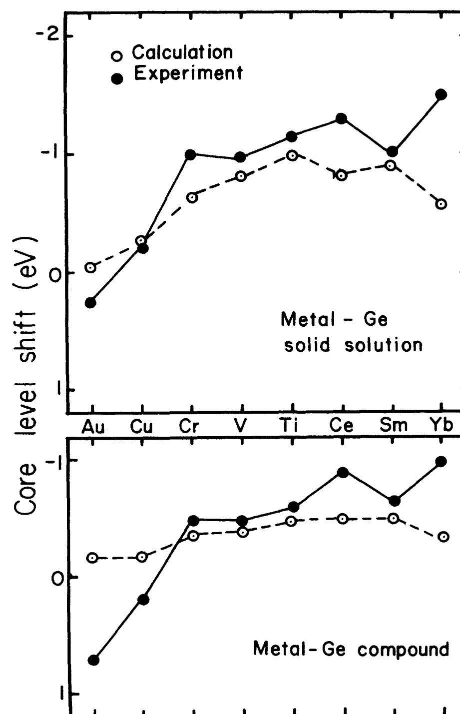

FIG. 5. Experimental and calculated Ge 3d CLS's for different metal overlayers. The top panel compares the trends for the solid solution phase while analogous comparisons for the first reacted phase are shown in the bottom. For the first phase we have assumed a CsCl structure and 50 at. % content in Si. Again, qualitatively good agreement is observed.

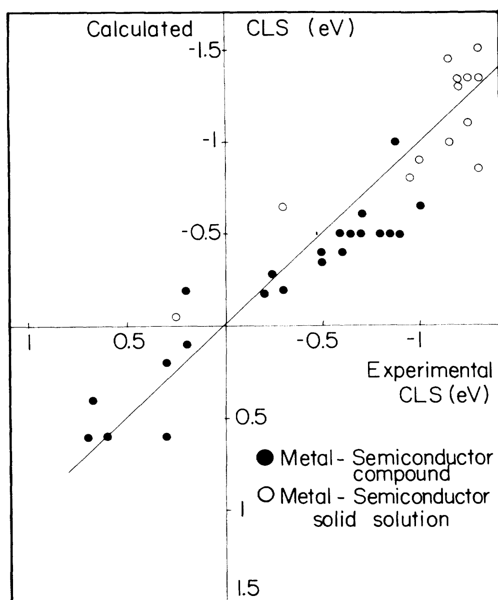

FIG. 6. Calculated vs experimental CLS's for the first reacted phase (closed symbols) and the solid solution (open symbols). Deviation from the line reflects disagreement between the calculation and the experiment.

heats of formation. First, when an *s-p* element is introduced into a transition-metal lattice, there is a lattice expansion to accommodate the impurity. This reduces the *d-d* overlap as the *d*-bands narrow and the cohesive energy is reduced, and the magnitude of the loss depends on the effective volume of the impurity. However, elements like Al and Si undergo variations in atomic volume when inserted in a transition metal to emulate the host volume (Turnbull rule).[52] This reduces the expansion energy contribution to the heat of formation, but parabolic variations across each transition-metal row are expected as a consequence of the *d*-bond strength dependence for these metals. A second and more important effect is related to the *d*-band hybridization with the *s* and *p* bands of solute. In a simplified approach, there will be bonding, nonbonding, and antibonding states once the *sp-d* bond is formed. By increasing the number of *d*-electrons going from Sc to Cu, for example, the bonding energy is lowered by filling the bonding states, there will be little change in bonding energy as the nonbonding states are filled, and there will be an energy increase as the antibonding states are filled. We then expect a parabolic behavior for the heats of formation across each transition metal row. The same kind of behavior is expected when the *s-p* partner is changed, but the parabolic minimum for the heats of formation is dependent on the *s-p* species used and corresponds to the filling of the *p-d* covalent bond states. The Miedema model, as we have used it here, would predict more or less adequate values for the heats of formation of these binary systems (in particular the sign of the energies), but would not reproduce the chemical trends discussed above because the calculations cannot treat these hybridization or expansion energies.

The calculated results for the alloys provide encouraging agreement with experiment considering the assumptions on composition and structure of these reacted phases. As far as the composition is concerned, we expect relatively small variations in the chemical shifts for compositions around 50% Si or Ge content.[53] A different choice of the lattice structure would also modify the trend via Eq. (1). However, the "universal" behavior observed suggests that relatively small corrections are expected from structural energy contributions. This conclusion is supported also by the analogous behaviors observed for the solid solution and the compounds.

Finally, underlying the interpretation of these results for Si- and Ge-based systems is a model that can be extended to explain the Ga 3*d* behavior for metal-GaAs interfaces. Indeed, Ga atoms form solid solutions at room temperature, and the Ga 3*d* core shifts can be correlated to heats of solution. As discussed in Ref. 32, qualitative agreement between chemistry, thermodynamics, and morphology related properties of reacted metal-GaAs interfaces, can be obtained. Most important, a general description of reactive interfaces can follow as a result of their work and the present one.

In conclusion, we have shown that the Si and Ge core-level shifts observed at room temperature for a large variety of metal overlayers can be qualitatively derived with a simple model based on the thermodynamic properties of the constituents. The chemical shifts have been calculated and interpreted through a structural model that connects interface morphology, diffusion, and reaction processes. Both solid solutions and compound formation have been considered. Extension to cases where two reacted compoundlike species are present is straightforward. A discussion of the limitations of the model has also been presented, with particular emphasis on the aspects related to band theory calculations. Further progress can indeed derive from more complex calculations considering the structure of real compounds.

ACKNOWLEDGMENTS

Stimulating discussions with M. W. Ruckman, R. E. Watson, C. Capasso, and F. Boscherini are gratefully acknowledged. This work was supported by the Army Research Office under Contract No. ARO-DAAG29-84-K-0169.

[1]L. J. Brillson, Surf. Sci. Rep. **2**, 123 (1982).
[2]C. Calandra, O. Bisi, and G. Ottaviani, Surf. Sci. Rep. **4**, 271 (1984).
[3]J. H. Weaver, in *Analysis and Characterization of Thin Films*, edited by K. N. Tu and R. Rosenberg (Academic, New York, 1987), Chap. 2.
[4]J. J. Joyce, M. Grioni, M. del Giudice, M. W. Ruckman, F. Boscherini, and J. H. Weaver, J. Vac. Sci. Technol. A **5**, 2019 (1987).
[5]J. H. Weaver, M. Grioni, J. J. Joyce, and M. del Guidice, Phys. Rev. B **31**, 5290 (1985); E. J. van Loenen, J. W. M. Frenken, and J. F. van der Veen, Appl. Phys. Lett. **45**, 41

(1984).

[6]L. J. Brillson, Thin Solid Films **89**, 461 (1982); J. L. Freeouf, J. Vac. Sci. Technol. **18**, 910 (1981); L. J. Brillson, C. F. Brucker, A. D. Katnani, N. G. Stoffel, R. R. Daniels, and G. Margaritondo, Surf. Sci. **132**, 212 (1983).

[7]G. W. Rubloff, Surf. Sci. **132**, 268 (1983); P. S. Ho, J. Vac. Sci. Technol. A **1**, 745 (1983).

[8]K. N. Tu and J. W. Mayer, in *Thin Films—Interdiffusion and Reaction,* edited by J. M. Poate, K. N. Tu, and J. W. Mayer (Wiley, New York, 1978), p. 359.

[9]R. Ludeke, J. Vac. Sci. Technol. B **2**, 400 (1984).

[10]*Epitaxial Growth,* edited by J. W. Matthews (Academic, New York, 1975), Vols. A and B.

[11]J. L. Robbins, Surf. Sci. **86**, 1 (1979).

[12]L. L. Chang, J. Vac. Sci. Technol. B **1**, 120 (1983).

[13]A. J. Noreika, M. H. Fracombe, and C. E. Wood, J. Appl. Phys. **52**, 7416 (1981).

[14]S. B. Whitehouse, C. T. Foxon, and B. A. Joyce, Appl. Phys. A **26**, 27 (1981).

[15]R. Ludeke, T. C. Chiang, and T. Miller, J. Vac. Sci. Technol. B **1**, 581 (1983); F. Xu, M. W. Ruckman, H.-W. Chen, J. J. Joyce, F. Boscherini, D. M. Hill, S. A. Chambers, and J. H. Weaver, Phys. Rev. B **35**, 2375 (1987); G. A. Prinz, Phys. Rev. Lett. **54**, 1051 (1985).

[16]J. H. Weaver, M. Grioni, and J. J. Joyce, Phys. Rev. B **31**, 5384 (1985).

[17]R. R. Daniels, A. D. Katnani, T. Xiu-Zhao, G. Margaritondo, and Z. Zunger, Phys. Rev. Lett. **49**, 895 (1982).

[18]M. Grioni, J. J. Joyce, S. A. Chambers, D. G. O'Neill, M. del Giudice, and J. H. Weaver, Phys. Rev. Lett. **53**, 2331 (1984); M. Grioni, J. J. Joyce, M. del Giudice, D. G. O'Neill, and J. H. Weaver, Phys. Rev. B **20**, 7370 (1984).

[19]M. del Giudice, J. J. Joyce, M. W. Ruckman, and J. H. Weaver, Phys. Rev. B **32**, 5149 (1985).

[20]A. Zunger, Phys. Rev. Lett. **47**, 875 (1981).

[21]A. Fujimori, M. Grioni, and J. H. Weaver, Phys. Rev. B **33**, 726 (1986).

[22]M. del Giudice, R. A. Butera, J. J. Joyce, M. W. Ruckman, and J. H. Weaver, Mater. Res. Soc. Symp. Proc. **54**, 91 (1986); M. del Giudice, R. A. Butera, M. W. Ruckman, J. J. Joyce, and J. H. Weaver, J. Vac. Sci. Technol. A **4**, 879 (1986).

[23]R. M. Tromp, G. W. Rubloff, and E. J. van Loenen, J. Vac. Sci. Technol. A **4**, 865 (1986); S. A. Chambers, D. M. Hill, F. Xu, and J. H. Weaver, Phys. Rev. B **35**, 634 (1987).

[24]S. M. Hu, in *Atomic Diffusion in Semiconductors,* edited by D. Shaw (Plenum, New York, 1973), p. 217.

[25]L. J. Brillson, A. D. Katnani, M. Kelly, and G. Margaritondo, J. Vac. Sci. Technol. A **2**, 551 (1984).

[26]A. Franciosi, D. G. O'Neill, and J. H. Weaver, J. Vac. Sci. Technol. B **1**, 3 (1983); A. Franciosi, D. W. Niles, G. Margaritondo, C. Quaresima, M. Capozi, and P. Perfetti, Phys. Rev. B **32**, 6917 (1985); see also Ref. 28.

[27]I. Abbati and M. Grioni, J. Vac. Sci. Technol. **19**, 631 (1981); F. Ringeissen, J. Derrien, E. Daugy, J. M. Layet, P. Mathiez, and F. Salven, J. Vac. Sci. Technol. B **1**, 546 (1983).

[28]P. S. Ho, P. E. Schmid, and H. Föll, Phys. Rev. Lett. **46**, 782 (1981); P. S. Ho, G. W. Rubloff, J. E. Lewis, V. L. Moruzzi, and A. R. Williams, Phys. Rev. B **22**, 4784 (1980).

[29]R. Purtell, A. Levi, G. Rubloff, and P. S. Ho, J. Vac. Sci. Technol. A **3**, 690 (1985).

[30]R. A. Butera, M. del Giudice, and J. H. Weaver, Phys. Rev. B **33**, 5435 (1986).

[31]A. Franciosi, D. J. Peterman, J. H. Weaver, and V. L. Moruzzi, Phys. Rev. B **25**, 4981 (1982).

[32]J. Nogami, T. Kendelewicz, I. Lindau, and W. E. Spicer, Phys. Rev. B **34**, 669 (1986).

[33]For some interfaces (Ti/Si and Ce/Ge, for example) another component has been observed at ultralow coverages. This component is associated with a Si-rich species. However, its presence does not affect the general arguments presented in this paper.

[34]M. del Giudice, J. J. Joyce, F. Boscherini, C. Capasso, and J. H. Weaver, Mater. Res. Soc. Symp. Proc. **77** (1987).

[35]M. del Giudice, J. J. Joyce, M. W. Ruckman, and J. H. Weaver, Phys. Rev. B **35**, 6213 (1987).

[36]M. del Giudice, M. Grioni, J. J. Joyce, M. W. Ruckman, S. A. Chambers, and J. H. Weaver, Surf. Sci. **168**, 309 (1986).

[37]F. Boscherini, J. J. Joyce, M. W. Ruckman, and J. H. Weaver, Phys. Rev. B **35**, 4216 (1987).

[38]Results for Pd/Si were obtained by M. del Giudice, F. Boscherini, C. Capasso, and J. H. Weaver (unpublished).

[39]The values reported are extracted from the Periodic Table of elements published by Sargent-Welch Scientific Company.

[40]G. Rossi, J. Nogami, I. Landau, L. Braicovich, I. Abbati, U. del Pennino, and S. Nannarone, J. Vac. Sci. Technol. A **1**, 781 (1983).

[41]C. D. Gelatt, J. R. Williams, and V. L. Moruzzi, Phys. Rev. B **27**, 2005 (1983).

[42]G. Hollinger, P. Kumurdjian, J. M. Mackowski, P. Pertosa, L. Porte, and Tran Minh Duc, J. Electron Spectrosc. **5**, 237 (1974).

[43]H. Bash, J. Electron Spectrosc. Relat. Phenom. **5**, 463 (1974).

[44]R. E. Watson, J. W. Davenport, M. L. Perlman, and T. K. Sham, Phys. Rev. B **24**, 1791 (1981); I. W. Davenport, R. E. Watson, M. L. Perlam, and T. K. Sham, Solid State Commun. **40**, 999 (1981).

[45]B. Johansson and N. Mårtensson, Phys. Rev. B **21**, 4427 (1980); P. H. Citrin and G. K. Wertheim, *ibid.* **27**, 3176 (1983).

[46]B. H. Verbeek, Solid State Commun. **44**, 951 (1982).

[47]A. R. Miedema, Z. Metallk. **70**, 345 (1979).

[48]A. R. Miedema, P. F. de Châtel, and F. R. de Boer, Physica **100B**, 1 (1980); A. K. Niessen, F. R. de Boer, R. Boom, P. F. de Châtel, W. C. M. Mattens, and A. R. Miedema, CALPHAD; Comput. Coupling Phase Diagrams Thermochem. **1**, 51 (1983).

[49]P. Perfetti, A. D. Katnani, T. Xiu-Zhao, and G. Margaritondo, J. Vac. Sci. Technol. **21**, 628 (1982); M. W. Ruckman, J. J. Joyce, F. Boscherini, and J. H. Weaver, Phys. Rev. B **34**, 5118 (1986).

[50]J. Nogami, C. Carbone, D. J. Friedman, and I. Lindau, Phys. Rev. B **33**, 864 (1986).

[51]A. R. Miedema, J. Less Common. Met. **46**, 67 (1976).

[52]D. Turnbull, Scripta Met. **11**, 1131 (1977); L. H. Bennett and R. E. Watson, Scripta Met. **16**, 1379 (1982).

[53]P. J. Grunthaner, F. J. Grunthaner, and A. Madhukar, J. Vac. Sci. Technol. **20**, 680 (1982).

[54]C. Carbone, J. Nogami, and I. Lindau, J. Vac. Sci. Technol. A **3**, 972 (1985).

[55]A. Franciosi, J. H. Weaver, P. Perfetti, A. D. Katnani, and G. Margaritondo, Solid State Commun. **47**, 427 (1983).

[56]O. Bisi and K. N. Tu, Phys. Rev. Lett. **52**, 1633 (1984).

[57]M. W. Ruckman, M. del Giudice, J. J. Joyce, and J. H. Weaver, Phys. Rev. B **34**, 410 (1986).

[58]A. Francisoi, P. Perfetti, A. D. Katnani, J. H. Weaver, and G. Margaritondo, Phys. Rev. B **29**, 5611 (1984).